PROCEEDINGS PAPER

Low-temperature crystal structures of the solvent dimethyl carbonate

Pamela S. Whitfield [a)]
Excelsus Structural Solutions (Swiss AG), Park Innovaare, Villigen, Switzerland

(Received 2 February 2023; accepted 17 February 2023)

Dimethyl carbonate (DMC) is an important industrial solvent but is additionally a common component of liquid lithium-ion battery electrolytes. Pure DMC has a melting point of 277 K, so encountering solidification under outdoor climatic conditions is very likely in many locations around the globe. Even eutectic, ethylene carbonate:dimethyl carbonate commercial $LiPF_6$ salt electrolyte formulations can start to solidify at temperatures around 260 K with obvious consequences for their performance. No structures for crystalline DMC are currently available which could be a hindrance for *in situ* battery studies at reduced temperatures. A time-of-flight neutron powder diffraction study of the phase behavior and crystal structures of deuterated DMC was undertaken to help fill this knowledge gap. Three different orthorhombic crystalline phases were found with a previously unreported low-temperature phase transition around 50–55 K. The progression of *Pbca* → *Pbcm* → *Ibam* space groups follow a sequence of group–subgroup relationships with the final *Ibam* structure being disordered around the central carbon atom.

[doi:10.1017/S088571562300009X]

Key words: non-ambient diffraction, organic structures, structure determination, TOF neutron diffraction

I. INTRODUCTION

Dimethyl carbonate (DMC) is an important chemical for the chemical industry, used as a methylating agent and as a volatile organic compound (VOC) exempt solvent. Its high dielectric constant, chemical stability and ability to dissolve ethylene carbonate made it one of the more common solvents used in commercial lithium-ion battery electrolytes. It has a relatively high melting point of 277 K and even when in a eutectic mixture with ethylene carbonate freezes out around 266 K (Ding et al., 2000). This has obvious implications for the conductivity of the electrolyte at low temperature and subsequent impact on the operation of any battery using such a DMC-containing electrolyte in a cold climate. Consequently, the structure and phase behavior of solid dimethyl carbonate are of particular interest when studying low-temperature performance of electrolytes. A literature calorimetry study (Ding et al., 2001) identified a solid–solid phase transition at around 210 K, so a diffraction study of crystalline DMC is expected to reveal at least one phase transition.

A study of DMC using a custom liquid nitrogen cryostream cooler between 90 K and room temperature with a laboratory X-ray powder diffractometer (Whitfield and Davidson, 2010) did indeed find a phase transition in the temperature region identified by Ding et al. (2001). Despite the addition of ground quartz inside the 1 mm quartz capillary as additional nucleating sites, data from repeated crystallizations were not reproducible and appeared to exhibit severe preferred orientation. Indexing could be carried out and a potential structure subsequently identified from the data collected at 90 K, but attempts using data above the phase transition were not successful.

Even with prior studies of other systems where data were reproducible (Whitfield et al., 2008), the preferred orientation induced via *in situ* crystallization with the laboratory instrumentation was significant. The co-axial cooling and subsequent temperature gradient was a likely contributing factor. The large sample volumes and differing sample environments at neutron facilities offered a potential way to manage such problems. The increased thermal mass of a larger sample could adversely affect the achievable cooling rate, leading to larger crystallites, but it was felt the improved particle statistics may lead to an overall improvement in data quality. A fully deuterated sample of DMC was chosen for the neutron experiment in order to avoid the data-degrading, incoherent scattering from a hydrogenous sample. Neutron facilities routinely make use of cryogenic sample environments, so the sample temperatures achievable are much lower than those via a liquid nitrogen cryostream cooler.

II. EXPERIMENTAL

The data were collected using the POWGEN time-of-flight (TOF) neutron powder diffractometer at the Spallation Neutron Source, Oak Ridge National Laboratory, USA (Huq et al., 2019). The 2 g sample of 99 atom% enriched d_6-DMC (CDN isotopes, Quebec, Canada) inside a helium-backfilled 6 mm vanadium can was crystallized *in situ* with silica aerogel as a nucleating agent dispersed in the liquid. The PAC 24-position sample changer was utilized with an accessible design temperature range of 8–300 K. A 1 Å

[a)]Author to whom correspondence should be addressed. Electronic mail: whitfieldps1@gmail.com

wide band centered on 1.5 Å yielded an accessible *d*-spacing range of 0.49–14.5 Å. Non-isothermal data were collected using a 1 K per minute ramp rate utilizing neutron event-mode temperature-binning (Granroth et al., 2018) to map the phase transitions. Isothermal datasets were collected at selected temperatures for improved statistics for refinement and to minimize thermal gradients.

The analyses of the diffraction data were carried out using TOPAS version 6 (Coelho et al., 2011). Indexing of the raw data was done using iterative least-squares LSI-index (Coelho, 2003). Simulated annealing using a z-matrix rigid body with idealized bond angles was used to find the starting structure model for refinement. A preferred orientation correction was applied during the simulated annealing as previously described by Whitfield (2009). Refinements maintained the z-matrix description with the addition of bond rotations where they were desirable for the particular structure. Refinement fits are displayed using the pdCIFplotter program (Rowles, 2022) from generated pdCIF files. Refined parameters included the scale factor, cell parameters, peak broadening, background, D/H ratio (ordered phases only), symmetry-allowed distortions, sample displacement (DIFA), and isotropic displacement parameters. Element B_{iso} values were restrained following the overall C_{2v} symmetry of the DMC molecule. A number of single peaks were used to assist in modeling the elevated background of the disordered *Ibam* phase.

Density functional theory (DFT) fixed unit cell optimization of the ordered structures were carried out using version 7 of the Quantum Espresso (Giannozzi et al., 2017) plane-wave code with the B3LYP hybrid functional with DFT-D3 dispersion correction (Grimme et al., 2010). Final refinements of the DFT-optimized structures described as z-matrices were carried out versus the experimental diffraction data. The DFT-optimized molecular conformation was utilized for the z-matrix rigid bodies for all the other refinements with that specific space-group. The refinement for the disordered *Ibam* structure used the DFT-optimized z-matrix conformation from the ordered *Pbam* structure.

III. RESULTS AND DISCUSSION

The sample crystallized immediately upon loading into the sample environment. On examination of the final data (Figure 1), it became apparent that there was an additional, previously unreported phase transition at a lower temperature than accessible with a liquid nitrogen cryostream. The candidate space-groups for each phase with increasing temperature were *Pbca*, *Pbcm*, and *Ibam*. Pawley refinements of the binned non-isothermal data showed a progressive increase in normalized cell volume with increasing temperature (Figure 2). The space groups are related by group–subgroup relationships so both 1st and 2nd order transitions are allowed via Landau theory (Landau, 2008).

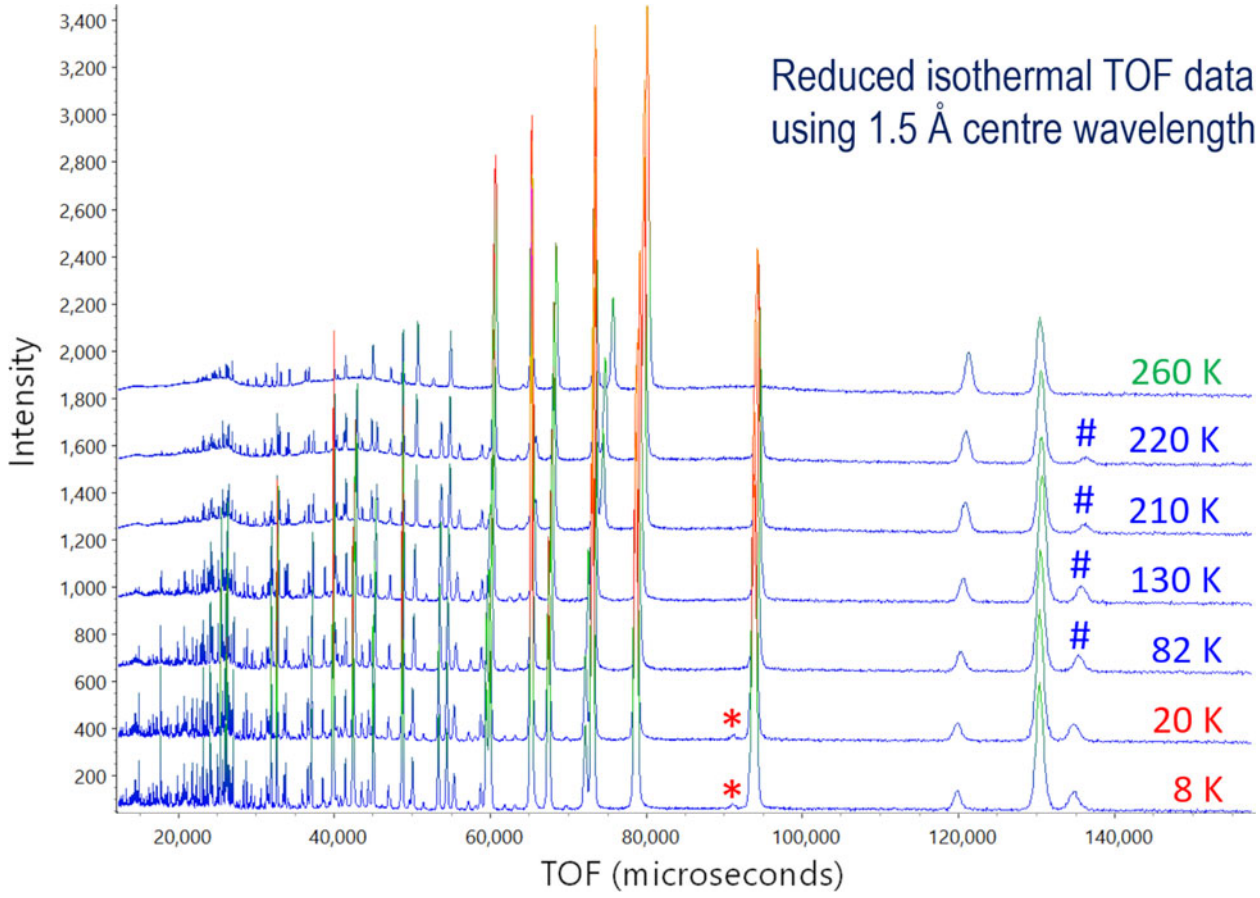

Figure 1. Stacked plot showing isothermal TOF data at different indicated temperatures for d_6-dimethyl carbonate. The different color labels designate the different structures to highlight the transitions. * marks a reflection that disappears in the *Pbca* → *Pbcm* phase transition, and # marks a corresponding reflection for the *Pbcm* → *Ibam* phase transition.

https://doi.org/10.1017/S088571562300009X Published online by Cambridge University Press

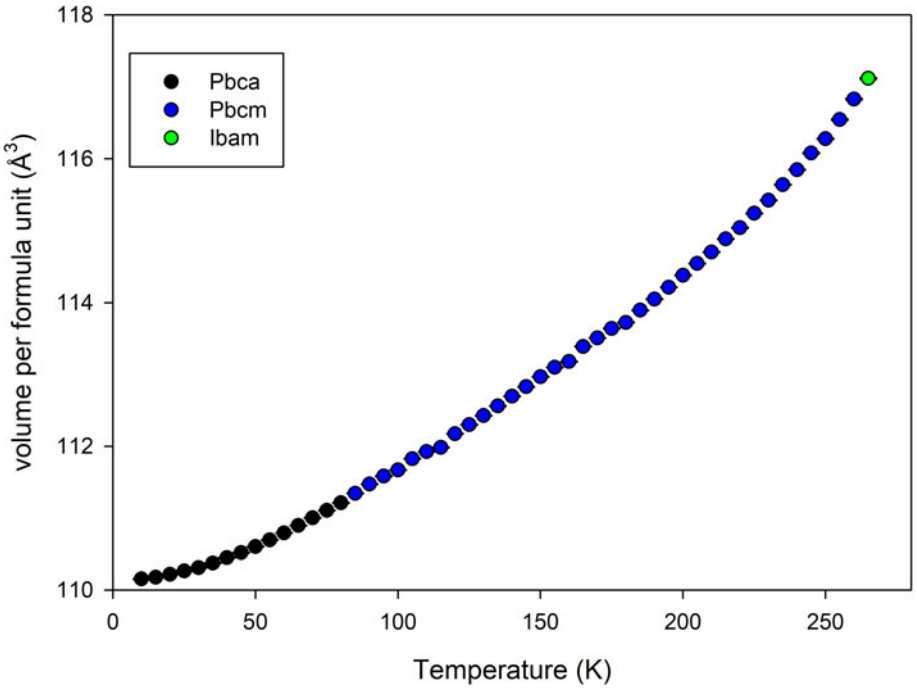

Figure 2. Volume per formula unit from Pawley refinement of non-isothermal data collected on heating at 1 K per minute between 10 and 270 K binned every 5 K.

With TOF data, it would have been desirable to extract anisotropic displacement parameters (ADPs), and to this end a refinement with the 8 K dataset using Translation-Libration-Screw (TLS) restraints (Schomaker and Trueblood, 1968) was attempted. The ellipsoids from this refinement under best possible conditions were unreasonably oblate, so isotropic displacement parameters were used throughout in results presented. The high degree of intensity

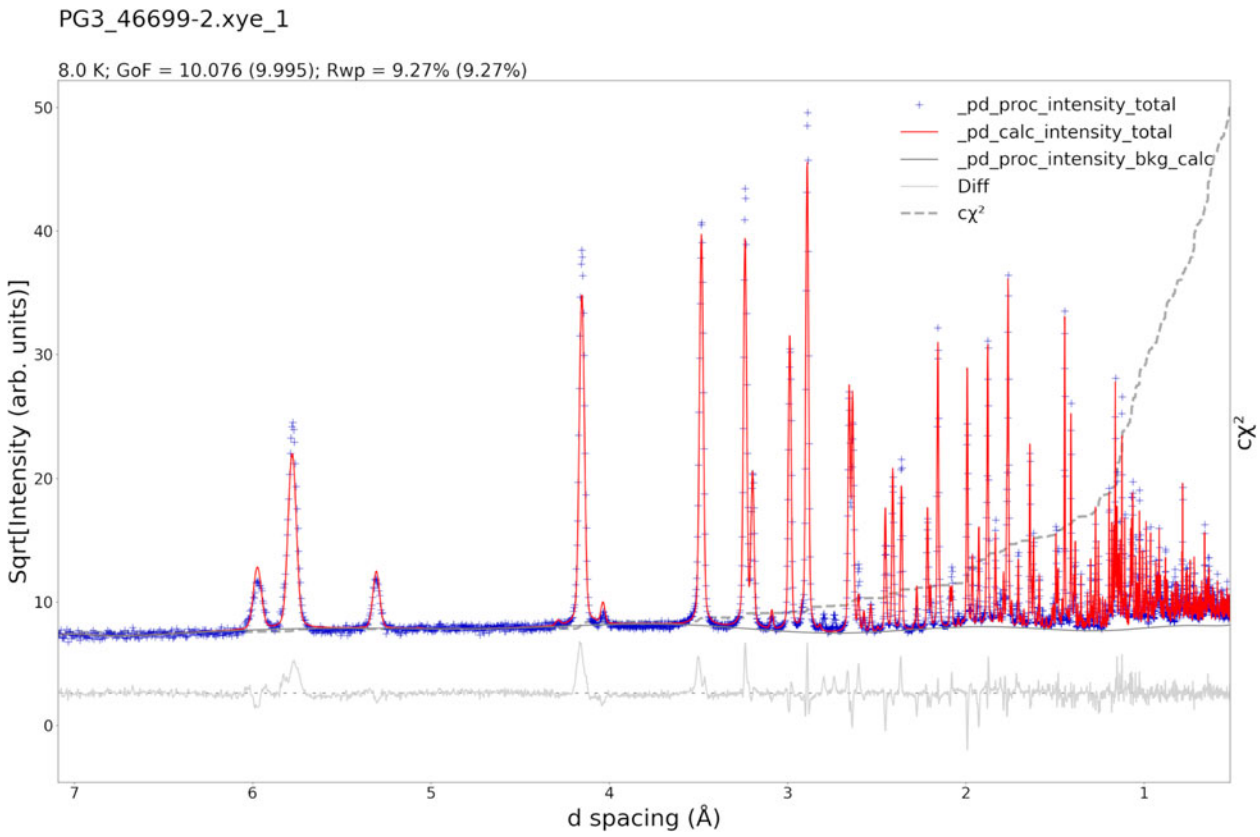

Figure 3. Refinement fit for the *Pbca* structure at 8 K.

https://doi.org/10.1017/S088571562300009X Published online by Cambridge University Press

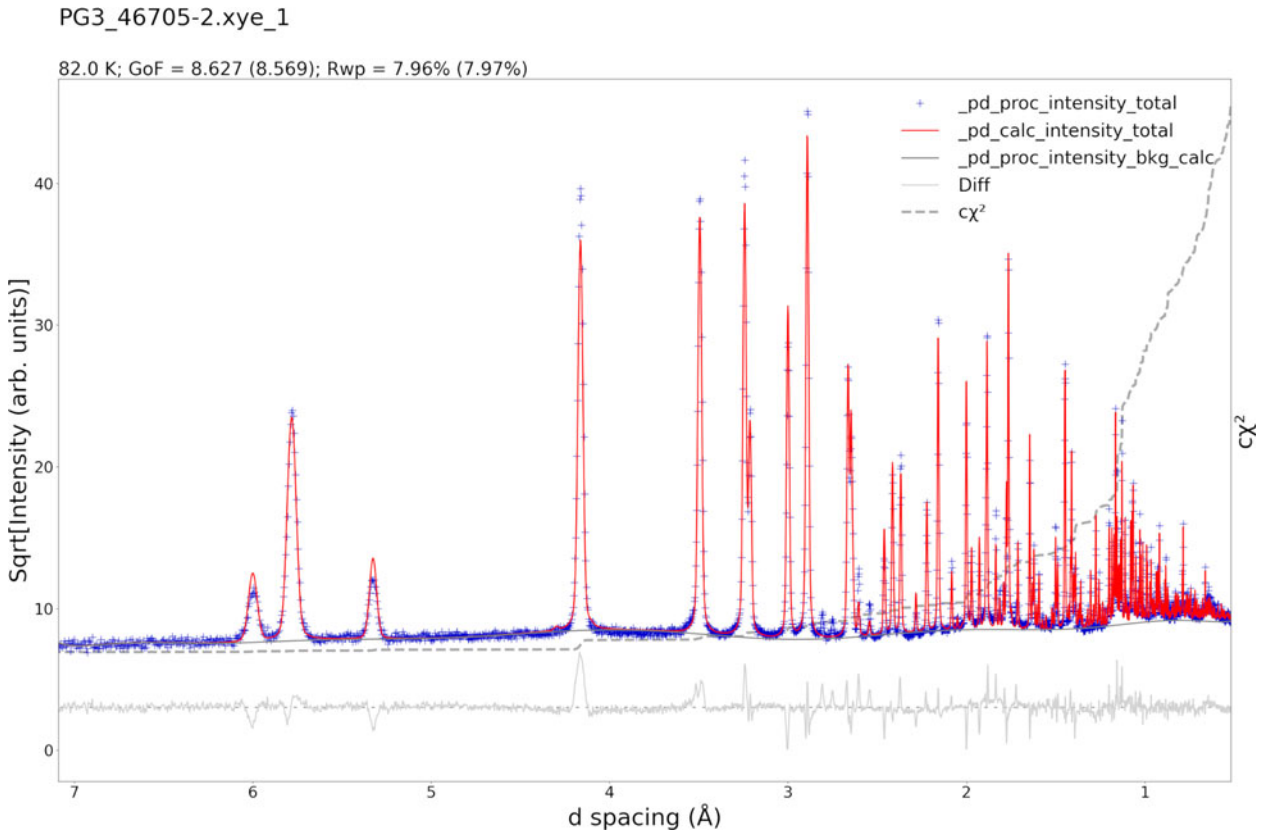

Figure 4. Refinement fit for the *Pbcm* structure at 82 K.

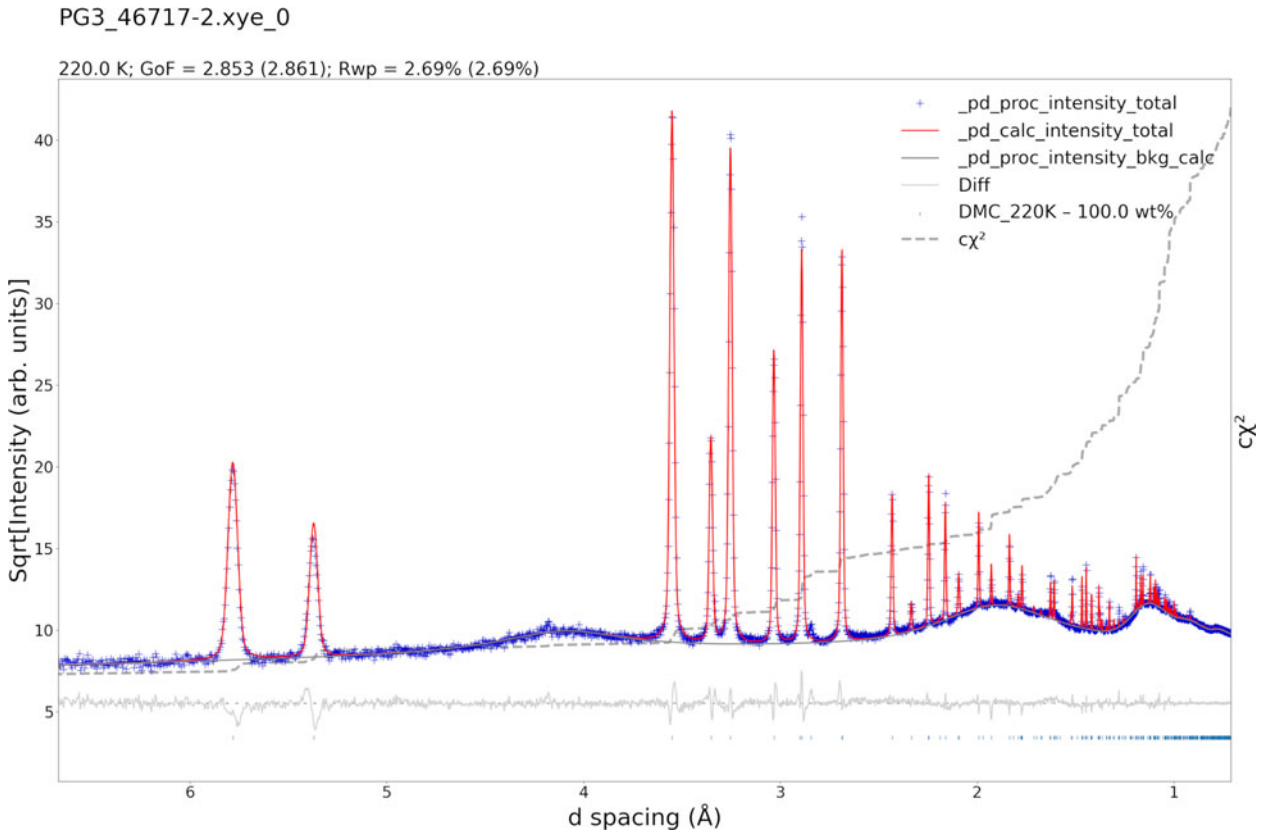

Figure 5. Refinement fit of the *Ibam* structure versus the data at an indicated temperature of 260 K. See main text for discussion about possible temperature calibration issue for this dataset.

https://doi.org/10.1017/S088571562300009X Published online by Cambridge University Press

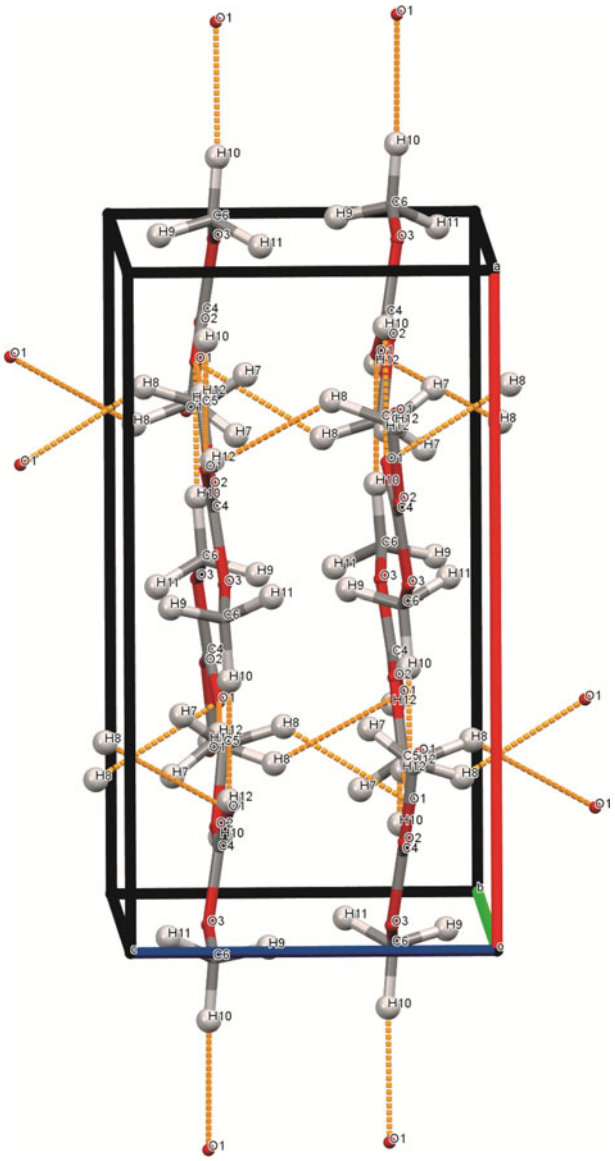

Figure 6. View of the low-temperature *Pbca* crystal structure of d_6-DMC refined using data at 8 K. The intermolecular C–H···O hydrogen bonds are indicated using the dashed orange lines. The isotropic displacement parameters are plotted at 50% probability. The deuterium atoms are labelled "H" to improve compatibility with the drawing package.

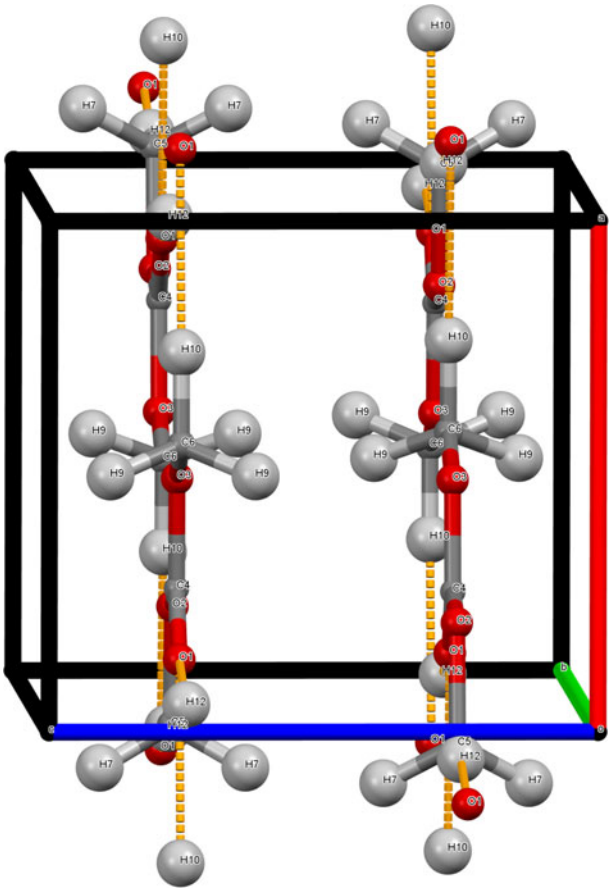

Figure 7. View of the intermediate temperature *Pbcm* crystal structure of d_6-DMC refined using data at 82 K. The intermolecular C–H···O hydrogen bonds are indicated using the dashed orange lines. The isotropic displacement parameters are plotted at 50% probability. The *a* lattice direction is orientated vertically to match Figure 6.

correlations with the spherical harmonics preferred orientation coefficients probably contribute to the inability to extract reasonable ADPs. The texture in the samples as indicated by the texture indices (Bunge, 1982, 88–90) was very high as was found previously with the laboratory X-ray data, but the larger volume of sample for the neutron data significantly improved the particle statistics.

The Rietveld refinement difference plots for the data collected at 8, 82, and 260 K are shown in Figures 3–5 as produced by the pdCIFplotter program (Rowles, 2022). The backgrounds with increasing sample temperature exhibit the expected growth of broad, periodic features in the low *d*-spacing region from thermal diffuse scattering. The higher backgrounds impact the calculated R_{wp} residual, contributing to the much lower R_{wp} value for the 260 K data refinement in Figure 5. The fits are reasonable but not as good as usually obtained with TOF neutron data. The suspicion is that the poor particle statistics with large crystallites observed in the earlier X-ray study with non-deuterated h_6-DMC (Whitfield and Davidson, 2010) also occurred with the neutron samples, although limited beamtime made repeated crystallization cycles as carried out during the X-ray study impossible. The X-ray study using transparent capillaries during crystallization allowed for observation of the resulting large, elongated crystallites via the alignment scope, but no such observations were possible inside opaque vanadium sample cans within the PAC sample changer. It should be noted that the design characteristics of POWGEN produce powder diffraction datasets with counting statistics heavily weighted to the backscattering detectors, i.e. at low *d*-spacing values. The cumulative χ^2 curves in Figures 3–5 are an indicator of this as the largest misfits visible in the difference plots have a minor effect on the least-squares minimization, the region < 1.5 Å having the largest impact.

The orthorhombic *Pbca* crystal structure refined from the 8 K data is shown in Figure 6. The molecules are arranged in a layered manner along the *c*-direction in an alternating manner to minimize steric interactions between the bulky methyl groups. No "conventional" hydrogen bonds involving hydroxide, amine, etc., can exist in the DMC structure. However, methyl hydrogens can and do form hydrogen bonds despite being far less polar (Steiner, 2002). C–H···O bonds with lengths ranging from around 2.3 to 2.6 Å and angles from

https://doi.org/10.1017/S088571562300009X Published online by Cambridge University Press

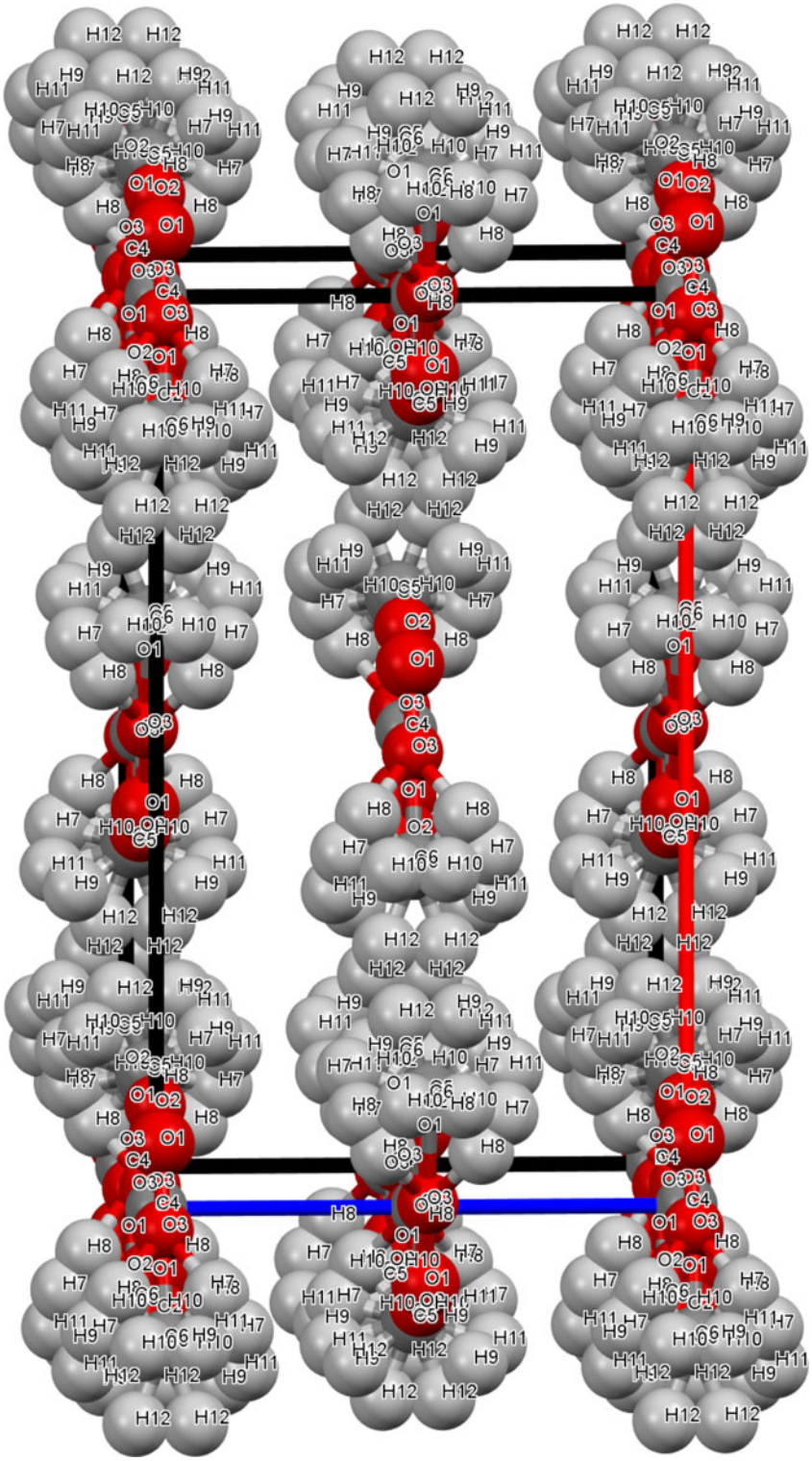

Figure 8. View of the high-temperature *Ibam* crystal structure of d_6-DMC refined using data at an indicated 260 K. See text for discussion about temperature calibration issue. The isotropic displacement parameters are plotted at 50% probability. The unit cell is orientated such that the *a* lattice direction is vertical to match Figures 6 and 7.

~120° to 175° occur in the 8 K DMC structure. The shorter and stronger interactions occur with adjacent molecules in the same *a*–*b* plane. Hydrogen bonds involving methyl groups are weaker and less directional than more "conventional" hydrogen bonds (Steiner, 2002). In the lowest energy structure, the DMC molecules arrange themselves so that two out of three hydrogens on each methyl group are weakly bonded to adjacent DMC molecules.

The *Pbcm* crystal structure refined using the 82 K data is shown in Figure 7. The arrangement in terms of alternating orientations along the *c*-direction is broadly similar to that of the *Pbca* structure except that the molecules now possess a mirror plane in the *a*–*b* plane. This leads to a halving of the *a* lattice parameter and reduction from eight DMC molecules in the unit cell to four. The hydrogen bond interactions with other molecules in the same *a*–*b* plane are largely unaffected but the longer-range C–H···O interactions tying the molecules together in the *c*-direction increase from ~2.6 Å at 8 K to ~2.9 Å, exceeding the sum of the van der Waals radii and effectively breaking the bonds.

https://doi.org/10.1017/S088571562300009X Published online by Cambridge University Press

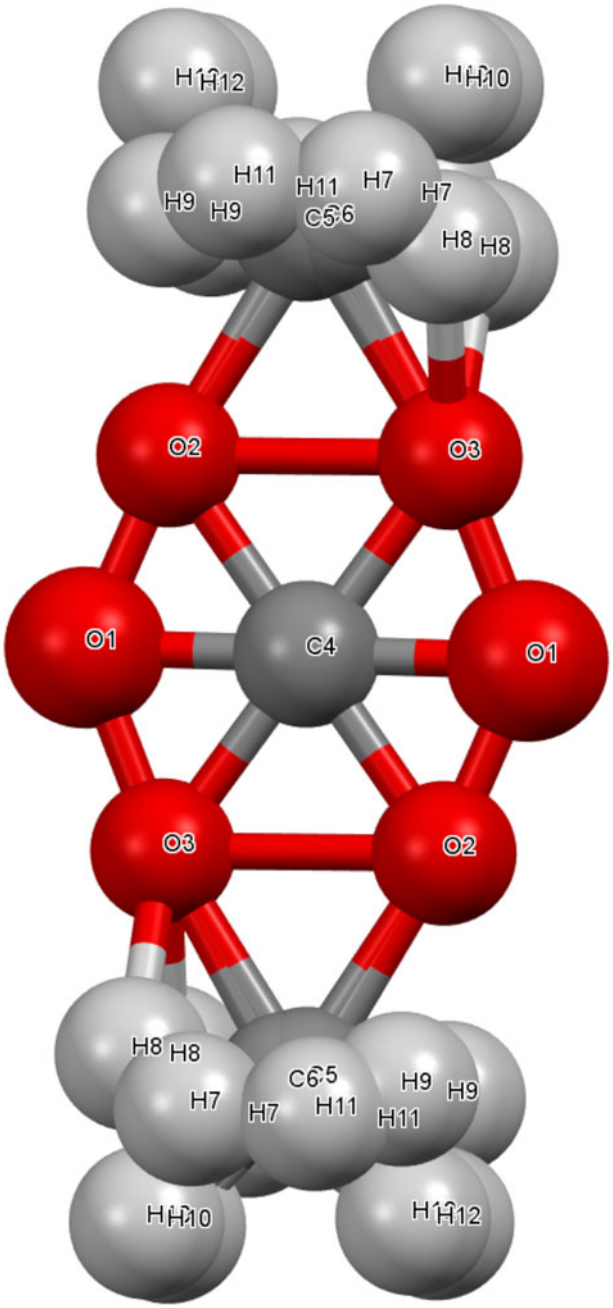

Figure 9. View of the disorder around the C(4) site in the high-temperature *Ibam* crystal structure of d_6-DMC. The isotropic displacement parameters are plotted at 50% probability.

The *Ibam* crystal structure refined using the 260 K data is shown in Figure 8. The sheer number and overlapping atomic sites hide the nature of the disorder of the DMC molecules so the disorder around a single C(4) atom is shown in Figure 9. The C(4) atom sits on the special 4*c* Wyckoff position. The disorder of the other non-deuterium atoms is generated by their 8-fold symmetry generator (8*j* Wyckoff position), while the almost spherical smearing of the deuterium atoms is symmetry-generated from their 16-fold general 16*k* positions. Each deuterium position is therefore only a quarter-occupied, effectively severing the already weak hydrogen bonding interactions between the DMC molecules. Given that sufficient energy was available to overcome the rotational barrier and flip the DMC molecule by 180° it is an interesting question as to whether a rotor model along the line C(5)–C(6) may be a realistic option, although the oxygen atoms of adjacent molecules would approach < 1 Å with full rotation. Using an approximate starting point via a rotation of the z-matrix by 45° and reducing the occupancies of the previously 8-fold atoms to 0.25 such a possibility was examined. The starting model did not fit the data and the structure quickly approached the previous planar geometry for the carbon and oxygen atoms of Figure 9. The refinement stabilized with a slightly improved R_{wp} of 2.47% and residual rotation of 13°, resulting in the disorder seen in Figure 10. The same effect of overlapping oxygen positions could be achieved using anisotropic thermal motion described with anisotropic displacement parameters without additional positional disorder. It is felt that the improvement in fit to the data was insufficient to warrant additional complexity in the proposed *Ibam* structure model.

In order to more clearly show the nature of the low-temperature phase transition, Figure 11 shows the *Pbca* (8 K) and *Pbcm* (82 K) structures aligned (viewed along the *b*-direction in both cases) with an overlapped region. The canting of the molecules that occurs on cooling through the low-temperature transition in clearly seen. This type of order–disorder transition is not uncommon and compatible with a continuous 2nd order phase transition. The *Pbca*–*Pbcm* transition occurs when the canting of the DMC molecule out of the *a*–*b* plane disappears. Figure 12 shows the rotation angle around the *Pbca b*-axis direction of the plane of the DMC molecule away from the unit cell *a*–*b* plane. The rotation angle reaches 0° between 45 and 50 K, indicating the phase transition occurs in this region. The exact temperature may be subject to minor error due to the 1 K per minute ramp rate used during collection of the parent dataset but not expected to exceed the 5 K temperature resolution (i.e. 5 min time resolution) in the extracted datasets.

Figure 13 shows a similar view to Figure 11 but highlighting the disorder in the *Ibam* (260 K) structure compared to the intermediate temperature *Pbcm* structure. The viewpoint in Figure 13 gives the illusion of 4-positional rotational disorder in the *Ibam* crystal structure which is not the case. The view in Figure 14 gives a more complete picture of the nature of the disorder in the *Ibam* phase. The disordered DMC units as seen previously in Figure 9 are stacked in an alternating manner in the *c*-direction with each rotated about 83° with respect to each other to minimize steric interactions between adjacent methyl groups.

Unfortunately, it became apparent that the sample environment used for the experiment had a significant nonlinear temperature calibration error that affected the higher temperature data in particular. The extent of the calibration error was such that the sample did not melt on heating to 300 K. The indicated sample environment temperature for the data of the high-temperature *Ibam* structure was 260 K. However, the *Pbcm* phase clearly persists in Figure 15 far above the known transition temperature of 210 K (Ding et al., 2001; Ding, 2004). It is estimated that the actual sample temperature for the *Ibam* refined data was 220–230 K. Some variation in melting point from an isotope effect is possible, but the expected difference in melting point between hydrogenous and deuterated DMC would be a maximum of 3–4 K rather than 30–40 K. It is understood that the calibration closer to the 8 K base temperature of the PAC sample changer had been checked for user magnetic structure studies using a

https://doi.org/10.1017/S088571562300009X Published online by Cambridge University Press

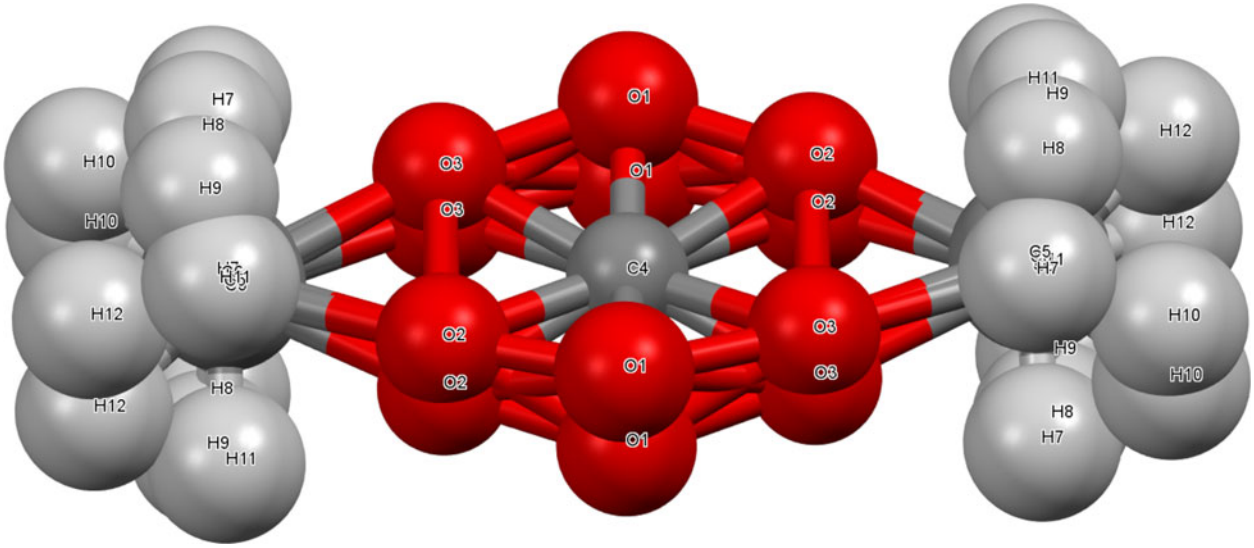

Figure 10. Resulting disorder when the DMC z-matrix is allowed to refine with a rotation along its long axis in the refinement of the *Ibam* structure. The isotropic displacement parameters are plotted at 50% probability.

low-temperature phase change material, but the calibration closer to ambient temperature had not been verified prior to user operations by SNS staff. Consequently, there is high confidence in the accuracy of the temperature for the 8 K data, and the indicated temperature for the 82 K data temperature is likely to be close. The final atomic coordinates for the 8, 82, and estimated 220 K structures are given in Tables I–III.

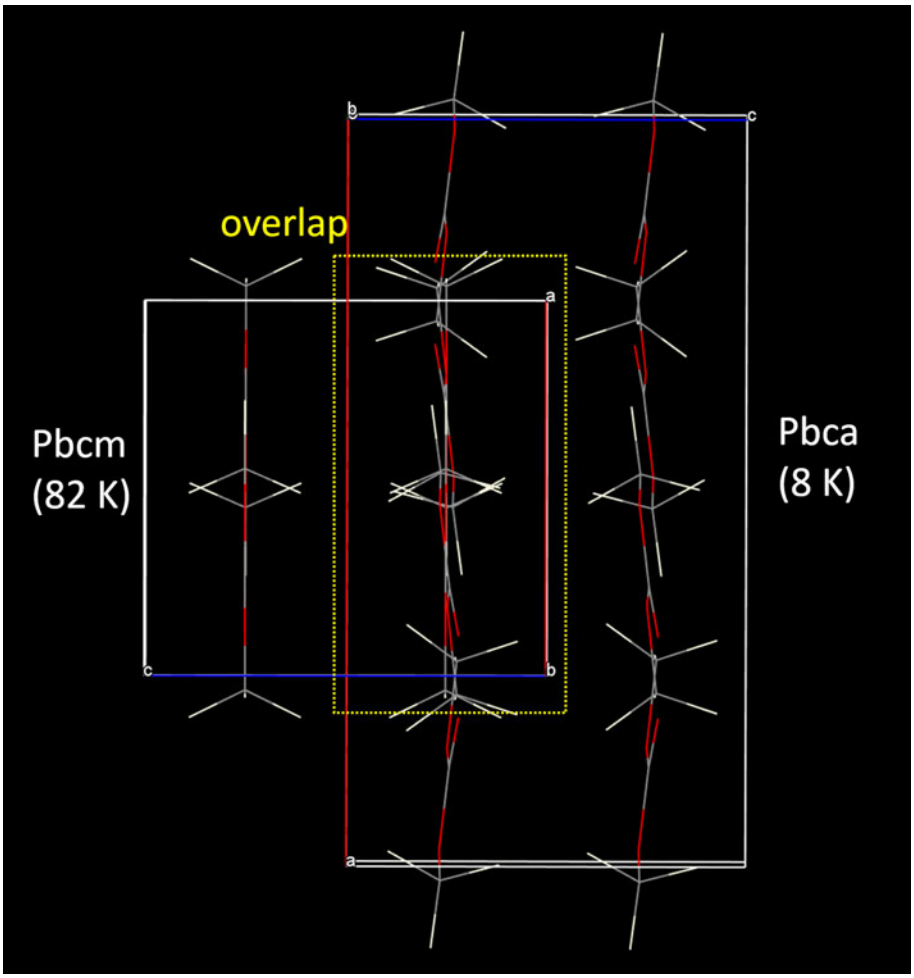

Figure 11. Representation showing how the *Pbca* structure relates to the *Pbcm* structure. Both crystal structures are viewed along the *b*-direction. The canting observed in *Pbca* (right) is replaced by a mirror plane in *Pbcm* (left).

https://doi.org/10.1017/S088571562300009X Published online by Cambridge University Press

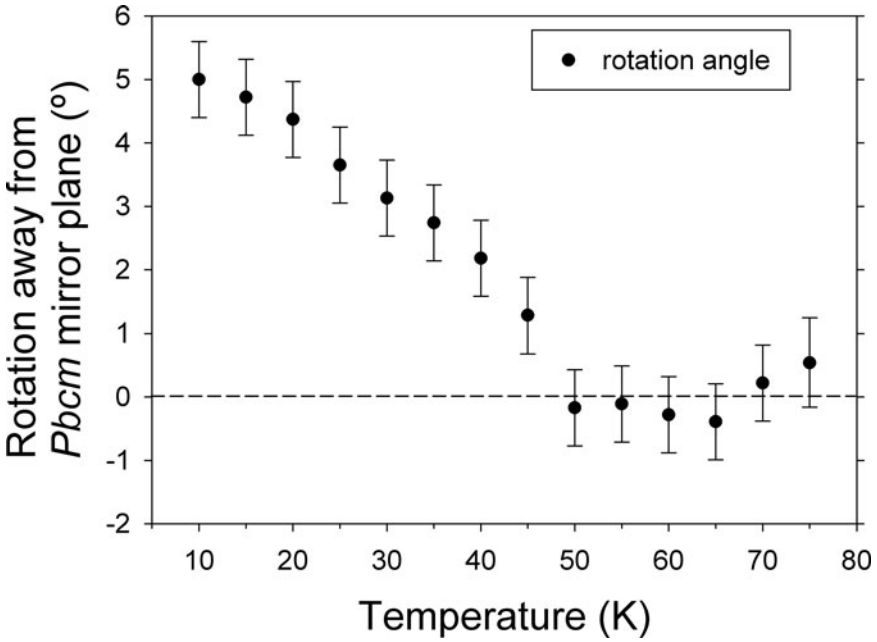

Figure 12. Rotation around the *b*-axis direction of the DMC molecule out of the *a*–*b* plane in the *Pbca* structure every 5 K using temperature-binned data. The *a*–*b* plane in *Pbca* corresponds to the mirror plane of the *Pbcm* space-group.

IV. CONCLUSION

A specimen of fully deuterated dimethyl carbonate has been crystallized successfully *in situ* inside the POWGEN time-of-flight neutron powder diffractometer, and diffraction data collected down to the base temperature of 8 K. Two phase transitions, the lower temperature transition previously unreported were observed. The three resulting crystal structures solved via simulated annealing prior to Rietveld refinement. The two ordered structures were optimized via density functional theory computation to provide the best possible intramolecular bond lengths/angles prior to a final refinement versus the data. The three crystalline phases follow sequential space-group relationships (*Pbca* → *Pbcm* → *Ibam*) with disorder increasing with temperature. The arrangement and distortion of the low-temperature ordered phases appear to be governed by weak hydrogen bonds between methyl-group deuterium atoms and oxygen atoms in adjacent

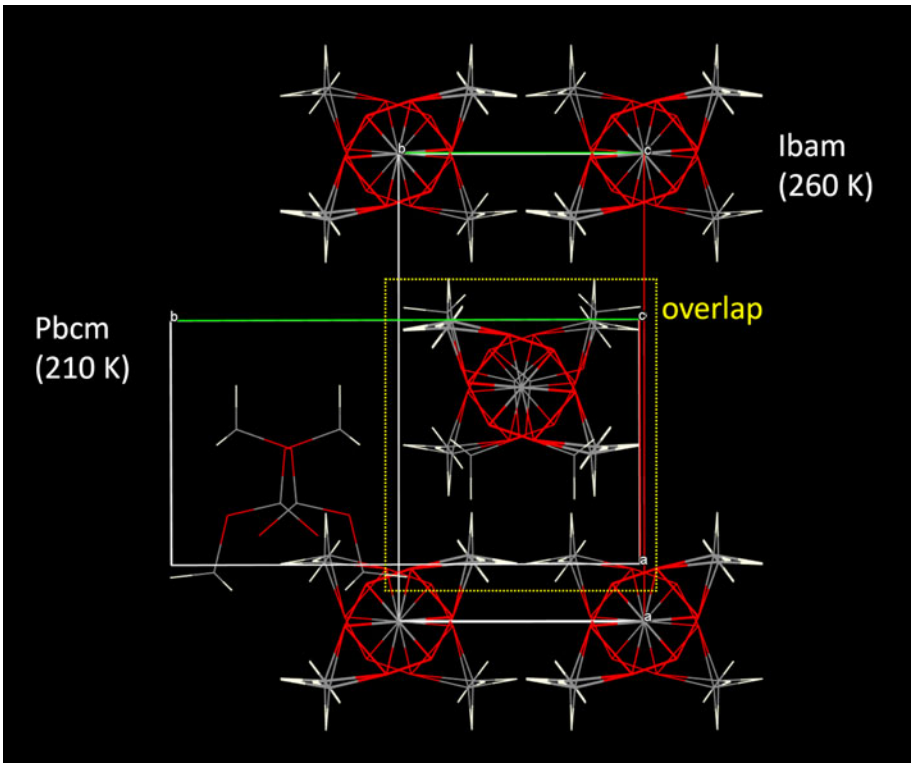

Figure 13. Representation showing how the *Pbcm* structure relates to the *Ibam* structure. In this instance, the *Pbcm* structure refined from a 210 K dataset is used for a closer match in temperature.

https://doi.org/10.1017/S088571562300009X Published online by Cambridge University Press

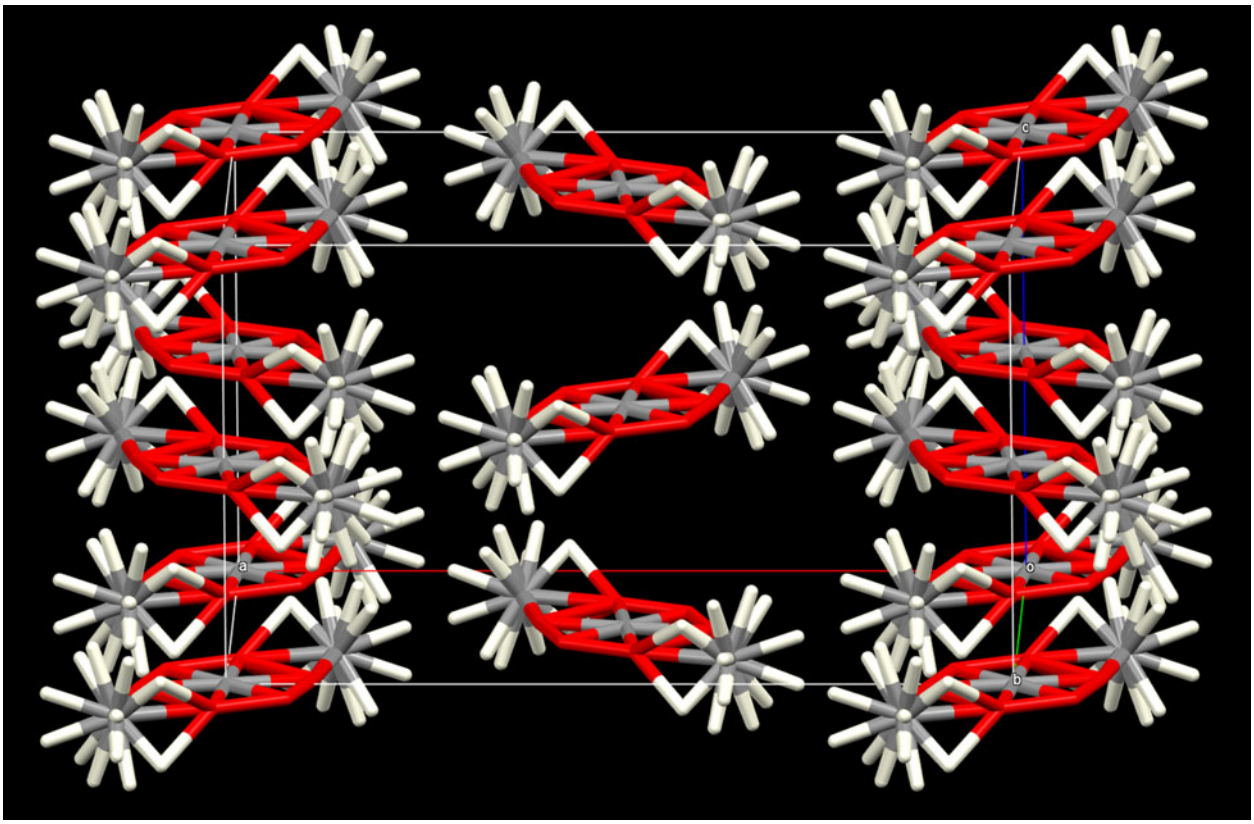

Figure 14. View of the *Ibam* structure highlighting the nature of the disorder within the unit cell and alternating orientation of the disordered DMC "units" when moving up in the *c*-direcion.

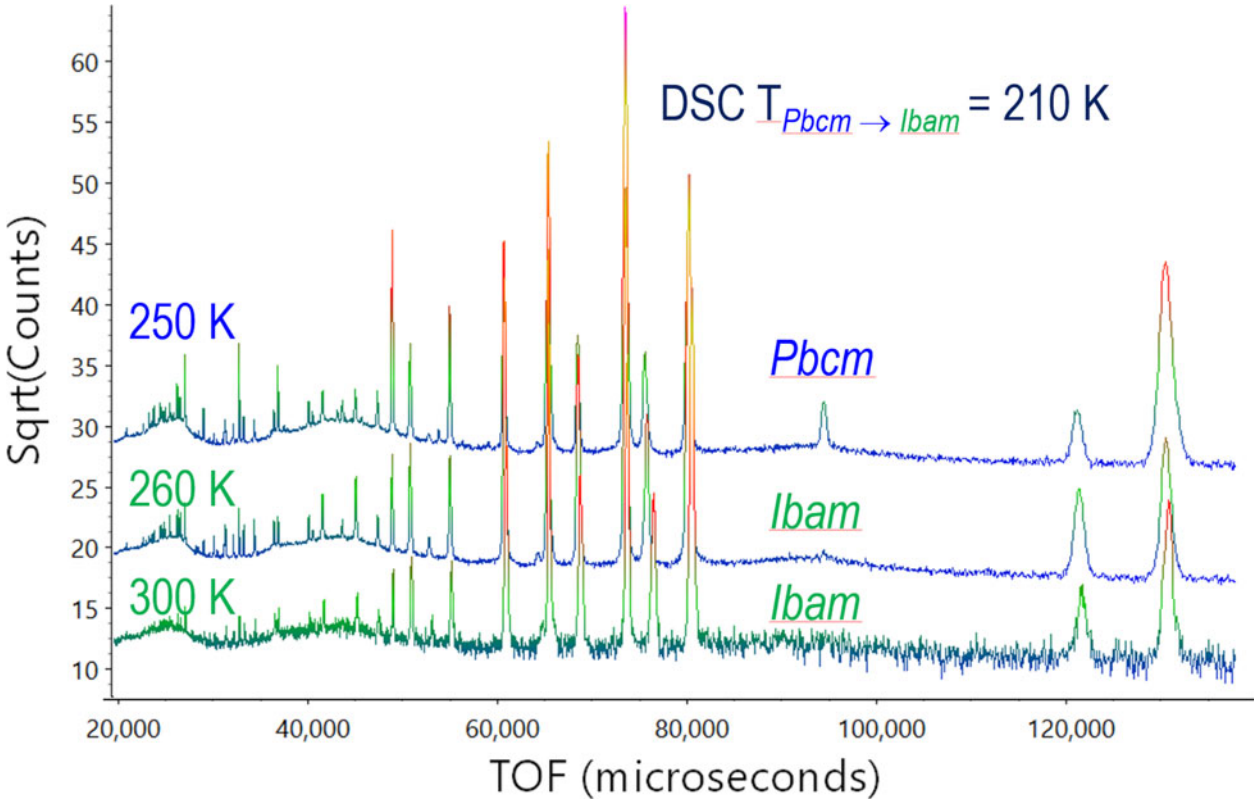

Figure 15. Closer examination of the raw data across the *Pbcm* to *Ibam* phase transition. The persistence of the *Pbcm* reflection at 95 000 μs demonstrates the deficiency in the temperature calibration in this regime closer to ambient conditions.

https://doi.org/10.1017/S088571562300009X Published online by Cambridge University Press

TABLE I. Atomic coordinates of d_6-DMC at 8 K.

Space group: *Pbca*, $Z = 8$, $Z' = 1$ $a = 11.9426(3)$ Å, $b = 11.5521$ (3) Å, $c = 6.3892(5)$ Å, $V = 881.47(8)$ Å^3 $\rho_x = 1.35774(9)$ g cm^{-3} Texture Index = 2.37(3) (Bunge, 1982, 88–90)					
T = 8 K atom	*x*	*y*	*z*	H_{occ}	B_{iso}
O(1)	0.1947(1)	0.30296(9)	0.2150(11)		0.34(6)
O(2)	0.1515(1)	0.10970(8)	0.2426(9)		0.50(4)
O(3)	0.0161(1)	0.2369(1)	0.2766(9)		0.50(4)
C(4)	0.12720(9)	0.22394(8)	0.2424(6)		0.22(5)
C(5)	0.2720(1)	0.0849(1)	0.2156(8)		0.51(4)
C(6)	−0.0239(1)	0.3579(1)	0.2687(8)		0.51(4)
D(7)	0.3188(2)	0.1256(4)	0.3428(10)	0.031(4)	1.62(4)
D(8)	0.3007(3)	0.1219(6)	0.0675(10)	0.031(4)	1.62(4)
D(9)	−0.0031(4)	0.3952(3)	0.1163(9)	0.031(4)	1.62(4)
D(10)	−0.1143(1)	0.3511(2)	0.2860(16)	0.031(4)	1.62(4)
D(11)	0.01368(5)	0.4072(3)	0.3968(12)	0.031(4)	1.62(4)
D(12)	0.2784(2)	−0.0090(1)	0.2149(16)	0.031(4)	1.62(4)

All total occupancies = 1.

TABLE II. Atomic coordinates of d_6-DMC at 82 K.

Space group: *Pbcm*, $Z = 4$, $Z' = 1$ $a = 5.9985(2)$ Å, $b = 11.5609$ (4) Å, $c = 6.4243(4)$ Å, $V = 445.51(4)$ Å^3 $\rho_x = 1.34236(10)$ g cm^{-3} Texture Index = 2.58(4) (Bunge, 1982, 88−90)					
T = 82 K atom	*x*	*y*	*z*	H_{occ}	B_{iso}
O(1)	0.8892(2)	0.80333(9)	0.25		1.28(8)
O(2)	0.8032(2)	0.61186(9)	0.25		1.11(5)
O(3)	0.5324(2)	0.7368(1)	0.25		1.11(5)
C(4)	0.7542(2)	0.72451(9)	0.25		0.73(5)
C(5)	1.0408(2)	0.5864(1)	0.25		1.10(4)
C(6)	0.4527(2)	0.8558(1)	0.25		1.10(4)
D(7)	1.0531(3)	0.4929(1)	0.25	0.035(4)	2.73(5)
D(8)	1.1168(2)	0.6229(1)	0.38864	0.035(4)	2.73(5)
D(9)	0.2726(2)	0.8484(2)	0.25	0.035(4)	2.73(5)
D(10)	0.5112(3)	0.9001(1)	0.38890	0.035(4)	2.73(5)

All total occupancies = 1.

TABLE III. Atomic coordinates of d_6-DMC at an estimated 220 K (260 K indicated).

Space group: *Ibam*, $Z = 4$, $Z' = 1$ $a = 11.5634(6)$ Å, $b = 6.0644(3)$ Å, $c = 6.7045(4)$ Å, $V = 470.16(4)$ Å^3 $\rho_x = 1.27242(11)$ Texture Index = 3.3(5) (Bunge, 1982, 88−90)						
T = 220 K (estimated) atom	*x*	*y*	*z*	occ	H_{occ}	B_{iso}
O(1)	1.07774(3)	−0.13158(7)	0	0.5		6.3(2)
O(2)	0.88909(1)	−0.04326(9)	0	0.5		5.1(1)
O(3)	1.01399(5)	0.21434(1)	0	0.5		5.1(1)
C(4)	1	0	0	1		5.2(1)
C(5)	0.86202(6)	−0.2751(1)	0	0.5		5.67(9)
C(6)	1.13298(7)	0.2882(1)	0	0.5		5.67(9)
D(7)	0.8817 (2)	−0.3488(1)	0.1389(1)	0.24124	0.00876	5.8(1)
D(8)	0.9234(3)	−0.3545(1)	−0.0925(7)	0.24124	0.00876	5.8(1)
D(9)	1.18159(8)	0.2096(4)	−0.1125(3)	0.24124	0.00876	5.8(1)
D(10)	1.1322(1)	0.4577(4)	−0.0518(9)	0.24124	0.00876	5.8(1)
D(11)	1.1634(2)	0.2743(10)	0.1521(2)	0.24124	0.00876	5.8(1)
D(12)	0.7776(2)	−0.2911(2)	−0.0565(8)	0.24124	0.00876	5.8(1)

Total occupancies = 1.

molecules. The *Pbca* → *Pbcm* transition coincides with the breaking of the weakest C–H···O hydrogen bonds between the molecule layers and the *Pbcm* → *Ibam* transition breaks all remaining intermolecular bonds. Despite some questions regarding the temperature calibration of the POWGEN sample environment closer to ambient conditions, the higher temperature *Ibam* crystal structure may prove particularly useful analyzing data from *in situ* lithium battery studies conducted under below-ambient conditions. However, the results seem to confirm previous observations that DMC has a tendency to crystallize with severe preferred orientation and potentially large crystallites making for a challenging sample for analysis via powder diffraction.

V. DEPOSITED DATA

The Crystallographic Information Framework (CIF) files were deposited with the ICDD. The data can be requested at pdj@icdd.com

ACKNOWLEDGEMENTS

This research used resources at the Spallation Neutron Source, a DOE Office of Science User Facility operated by the Oak Ridge National Laboratory.

The author would like to thank Dr Melanie Kirkham at the Spallation Neutron Source for her assistance in collecting the data remotely during one of the Covid-19 shutdowns.

CONFLICTS OF INTEREST

The author declares no conflicts of interest.

REFERENCES

Bunge, H. J. 1982. *Texture Analysis in Materials Science: Mathematical Methods*. Oxford, Butterworth-Heinemann.

Coelho, A. A. 2003. "Indexing of Powder Diffraction Patterns by Iterative Use of Singular Value Decomposition." *Journal of Applied Crystallography* 36 (1): 86–95. doi:10.1107/S0021889802019878.

Coelho, A. A., J. Evans, I. Evans, A. Kern, and S. Parsons. 2011. "The TOPAS Symbolic Computation System." *Powder Diffraction* 26 (S1): S22–5. doi:10.1154/1.3661087.

Ding, M. S. 2004. "Liquid-Solid Phase Equilibria and Thermodynamic Modelling for Binary Organic Carbonates." *Journal of Chemical Engineering Data* 49 (2): 276–82. doi:10.1021/je034134e.

Ding, M. S., K. Xu, and T. R. Jow. 2000. "Liquid-Solid Phase Diagrams of Binary Carbonates for Lithium Batteries." *Journal of the Electrochemical Society* 147 (5): 1688–94. doi:10.1149/1.1393419.

Ding, M. S., K. Xu, S. Zhang, and T. R. Jow. 2001. "Liquid-Solid Phase Diagrams of Binary Carbonates for Lithium Batteries. Part II." *Journal of the Electrochemical Society* 148 (4): A299–304. doi:10.1149/1.1353568.

Giannozzi, P., O. Andreussi, T. Brumme, O. Bunau, M. Buongirno, M. Calandra, R. Car, *et al*. 2017. "Advanced Capabilities for Materials Modelling with Quantum ESPRESSO." *Journal of Physics: Condensed Matter* 29 (46): 465901. doi:10.1088/1361-648X/aa8f79.

Granroth, G. E., K. An, H. L. Smith, P. Whitfield, J. C. Neuefeind, J. Lee, W. Zhou, *et al*. 2018. "Event-Based Processing of Neutron Scattering Data at the Spallation Neutron Source." *Journal of Applied Crystallography* 51 (3): 616–29. doi:10.1107/S1600576718004727.

Grimme, S., J. Antony, S. Ehrlich, and H. Krieg. 2010. "A Consistent and Accurate Ab Initio Parameterization of Density Functional Dispersion Correction (DFT-D) for the 94 Elements H-Pu." *Journal of Chemical Physics* 132 (15): 154104. doi:10.1063/1.3382344.

Huq, A., M. Kirkham, P. F. Peterson, J. P. Hodges, P. S. Whitfield, K. Page, T. Hügle, *et al*. 2019. "POWGEN: Rebuild of a Third-Generation Powder Diffractometer at the Spallation Neutron Source." *Journal of Applied Crystallography* 52 (5): 1189–201. doi:10.1107/S160057671901121X.

Landau, L. 2008. "On the Theory of Phase Transitions." *Ukrainian Journal of Physics* 53 (Special Issue): 25–35. (English translation of Zh. Eksp. Teor. Fiz. (1937), 7, 19–32).

Rowles, M. R. 2022. "pdCIFplotter: Visualizing Powder Diffraction Data in pdCIF Format." *Journal of Applied Crystallography* 55 (3): 631–7. doi:10.1107/S1600576722003478.

Schomaker, V., and K. N. Trueblood. 1968. "On the Rigid-Body Motion of Molecules in Crystals." *Acta Crystallographica B* 24 (1): 63–76. doi:10.1107/S0567740868001718.

Steiner, T. 2002. "The Hydrogen Bond in the Solid State." *Angewandte Chemie International Edition* 41 (1): 48–76. doi:10.1002/1521-3773(20020104)41:1%3C48::AID-ANIE48%3E3.0.CO;2-U.

Whitfield, P. S. 2009. "Spherical Harmonics Preferential Orientation Corrections and Structure Solution from Powder Diffraction Data – A Possible Avenue of Last Resort." *Journal of Applied Crystallography* 42 (1): 134–6. doi:10.1107/S0021889808041149.

Whitfield, P. S., and I. J. Davidson. 2010. "Low Temperature Phase Behaviour and Crystal Structures of Electrolyte Solvents And Additives" Presentation at the 15th International Meeting on Lithium Batteries, Montreal, QC, Canada, June 27–July 3, 2010.

Whitfield, P. S., Y. Le Page, A. Abouimrane, and I. J. Davidson. 2008. "Ab-Initio Structure Determination of the Low Temperature Phase of Succinonitrile from Laboratory X-Ray Powder Diffraction Data – Coping With Potential Poor Powder Quality Using DFT *Ab Initio* Methods." *Powder Diffraction* 23 (4): 292–9. doi:10.1154/1.3009635.